SCIENCE CHINA
Chemistry

• ARTICLES •

March 2012 Vol.55 No.3: 443–450
doi: 10.1007/s11426-012-4527-8

Cobalt(II) coordination polymers built on isomeric dipyridyl triazole ligands with pyromellitic acid: Synthesis, characterization and their effects on the thermal decomposition of ammonium perchlorate

XIE Gang[1], LI Bing[1,2], CHEN SanPing[1*], YANG Qi[1], WEI Wei[1] & GAO ShengLi[1*]

[1]*Key Laboratory of Synthetic and Natural Functional Molecule Chemistry of Ministry of Education; College of Chemistry and Materials Science, Northwest University, Xi'an 710069, China*
[2]*School of Chemistry & Chemical Engineering, Ningxia University, Yinchuan 750021, China*

Received December 5, 2011; accepted December 28, 2011

Three new cobalt(II) coordination compounds, $[Co(3,3'\text{-Hbpt})_2(H_2pm)(H_2O)_2]\cdot 2H_2O$ (**1**), $[Co(4,4'\text{-Hbpt})(pm)_{0.5}(H_2O)]\cdot 3H_2O$ (**2**) and $[Co(3,4'\text{-Hbpt})(pm)_{0.5}(H_2O)_3]\cdot 2H_2O$ (**3**) (3,3′-Hbpt = 3,5-bis(3-pyridyl)-1*H*-1,2,4-triazole; 4,4′-bpt = 3,5-bis(4-pyridyl)-1*H*-1,2,4-triazole, 3,4′-Hbpt = 3-(3-pyridyl)-5-(4′-pyridyl)-1*H*-1,2,4-triazole and H_4pm = pyromellitic acid) have been synthesized by hydrothermal reactions. Single-crystal X-ray diffraction reveals that compound **1** has a one-dimensional (1D) chain network, **2** exhibits a four-connected three-dimensional (3D) structure with 1D open channels encapsulated by water molecules, while **3** displays a regular two-dimensional (2D) architecture connected through 1D metal helical chains. In addition, the efficacy of compounds **1–3** as additives to promote the thermal decomposition of ammonium perchlorate (AP) is explored by differential scanning calorimetry (DSC).

cobalt(II) coordination compound, 3,5-bis-pyridyl-1*H*-1,2,4-triazole, combustion catalysis, ammonium perchlorate

1 Introduction

The design and assembly of metal–organic frameworks (MOFs) based on triazole and its derivatives are of great interest in materials science by virtue of their intriguing architectures and potential applications in luminescence, nonlinear optics, adsorption and magnetism [1–8]. Due to their high nitrogen content, triazole and its derivatives are also widely used as energetic materials [9–12]. As one of the derivatives of triazole, 3,5-bis-pyridyl-1-*H*-1,2,4-triazole serves as an *N*,*N*′-donor ligand and acts as a bridging ligand, thus mediating exchange coupling. Furthermore, the prototropy and conjugation between the 1*H*-1,2,4-triazole and pyridyl groups alter the electron density in different sections of the molecules, making the ligand more flexible [13, 14]. In addition, the different possible positions of the pyridyl nitrogen atoms endow the ligands (Scheme 1) with versatile coordination modes, facilitating the formation of different topological structures [15].

Ammonium perchlorate (AP) is the most common oxidizer in composite solid propellants and the thermal decomposition characteristics of AP directly influence the combustion behavior of such solid propellants [16, 17]. The reaction rate and pyrolysis temperature of the thermal decomposition of AP are closely related to the combustion rate of the solid propellants, with lower pyrolysis temperatures resulting in faster combustion rates.

In order to study the effects of compounds containing Hbpt on the thermal decomposition of AP, we chose cobalt(II) ions as the coordination center and pyromellitic acid

*Corresponding author (email: sanpingchen@126.com; gaoshli@nwu.edu.cn)

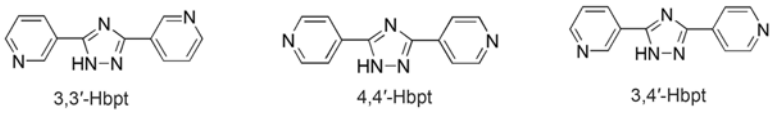

Scheme 1 The positionally isomeric bridging ligands.

(H_4pm) as an auxiliary ligand on the basis of the following considerations: (1) the cobalt(II) ion shows good catalytic performance for the decomposition of propellants [18]; (2) H_4pm can improve the oxygen balance of propellant components [19–21]. Moreover, H_4pm is a good candidate for the construction of MOFs through full or partial deprotonation [22–24]. In this paper, we report the syntheses and structures of three cobalt(II) coordination compounds with Hbpt isomers in the presence of the H_4pm ligand, namely, $[Co(3,3'\text{-Hbpt})_2(H_2pm)(H_2O)_2]\cdot 2H_2O$ (**1**), $[Co(4,4'\text{-Hbpt})(pm)_{0.5}(H_2O)]\cdot 3H_2O$ (**2**) and $[Co(3,4'\text{-Hbpt})(pm)_{0.5}(H_2O)_3]\cdot 2H_2O$ (**3**). Furthermore, the catalytic performances of **1–3** in the thermal decomposition of AP were explored.

2 Experimental

2.1 Materials

Commercially available reagents were used as received without further purification. Elemental analyses (C, H and N) were performed on a Vario EL III analyzer. Infrared spectra were obtained using KBr pellets on a BEQ VZNDX 550 FTIR instrument within the 400–4000 cm^{-1} region. ^1H NMR spectra were recorded on a Varian Inova 400 instrument using tetramethylsilane (TMS) as an internal standard. Thermal analyses were performed on a NETZSCH STA 449C instrument under an atmosphere of hydrostatic air at a heating rate of 10 °C min^{-1}. Differential scanning calorimetry (DSC) experiments were performed on a Perkin-Elmer Pyris 6 DSC thermal analyzer (calibrated using pure indium and zinc as standards) from 50 to 500 °C.

2.2 Synthesis of Hbpt

The 3,3′-Hbpt ligand was synthesized via an *in situ* metal/ligand reaction and demetallation as follows (Scheme 2): A mixture of 3-cyanopyridine (1.04 g, 10.0 mmol), aqueous ammonia (1.0 mL), $Cu(NO_3)_2\cdot 6H_2O$ (0.296 g, 1.0 mmol) and water (5 mL) was sealed in a 15 mL Teflon-lined autoclave and treated at 140 °C for 60 h. The resulting mixture was filtered to give crystalline $[Cu_2(bpt)_2]$ in 40% yield based on 3-cyanopyridine. The product then underwent a process of demetallation: The as-synthesized $[Cu_2(bpt)_2]$ was placed in a 200 mL flask containing 100 mL of water, into which 2 mL of ammonium sulfide solution was added dropwise with stirring. After 0.5 h, the solution was boiled and filtered to give a colorless solution and then concentrated to afford 3,5-bis(3-pyridyl)-1H-1,2,4-triazole (3,3′-Hbpt) (260 mg, 25.0% based on 3-cyanopyridine). Anal. calcd for $C_{12}H_9N_5$: C, 64.56; H, 4.06; N, 31.37. Found: C, 64.96; H, 4.40; N, 32.45%. Mp: 232–233 °C; IR (cm^{-1}, KBr): 3327(s), 3156(s), 3048(m), 2843(m), 1620(s), 1594(s), 1482(w), 1406(s), 1308(s), 1196(w), 1051(m), 821(m), 709(m), 625(w); ^1H NMR (400 MHz, DMSO-d_6, δ ppm): 7.534–7.552 (2H, m, J = 7.2 Hz), 8.408–8.427 (2H, d, J = 7.6 Hz), 8.723–8.743 (2H, dd, J = 8.0 Hz), 9.272(2H, s), 14.926 (1H, s, triazole-H).

The same procedure as that for the 3,3′-Hbpt ligand was used for the synthesis of 4,4'-Hbpt except that 3-cyanopyridine was replaced by 4-cyanopyridine. (Yield: 420 mg, 40.3% based on 4-cyanopyridine). Mp: 296–297 °C; Anal. calcd for $C_{12}H_9N_5$: C, 64.56; H, 4.06; N, 31.37. Found: C, 64.85; H,4.09; N, 33.04%. IR (cm^{-1}, KBr): 3408(w), 3088(m), 2623(m),1606(s), 1580(s), 1447(m), 1423(m), 1378(m), 1362(m), 1152(s), 1015(m), 987(m), 832(s), 720(m), 709(m), 528(s); ^1H NMR (400 MHz, DMSO-d_6, δppm): 8.010–8.025 (4H, d, J = 6.0 Hz), 8.768–8.779 (4H, d, J = 4.4 Hz), 15.232 (1H, s, triazole-H).

3,4′-Hbpt was synthesized according to ref. [25] and characterized by IR and elemental analysis. Anal. calcd for $C_{12}H_9N_5$: C, 64.56; H, 4.06; N, 31.37. Found: C, 64.88; H,4.56; N, 32.88%. Mp: 240–241 °C; IR (cm^{-1}, KBr): 3408(w), 3088(m), 2623(m), 1606(s), 1580(s), 1447(m), 1423(m), 1378(m), 1362(m), 1152(s), 1015(m), 987(m), 832(s), 720(m), 709(m), 528(s); ^1H NMR (400 MHz, DMSO-d_6, δ ppm): 6.951–6.980 (1H, d, J = 11.6 Hz), 7.508–7.539 (1H, m, J = 12.4 Hz), 7.797–7.810 (2H, d, J = 5.2 Hz), 8.220–8.240 (1H, d, J = 8.0 Hz), 8.662–8.674 (2H, d, J = 4.8 Hz), 9.054 (1H, s); 10.329 (1H, s, triazole-H).

2.3 Synthesis of $[Co(3,3'\text{-Hbpt})_2(H_2pm)(H_2O)_2]\cdot 2H_2O$ (1)

A mixture containing cobalt(II) acetate ($Co(OAc)_2\cdot 4H_2O$) (12.4 mg, 0.05 mmol), 3,3′-Hbpt (11.2 mg, 0.05 mmol), H_4pm (12.7 mg, 0.05 mmol) and water (6 mL) was sealed in a 15 mL Teflon-lined stainless steel vessel and heated at 140 °C for 3 days and then cooled to room temperature at a rate of 5 °C/h. Red prismatic crystals of **1** were collected in a yield of 50% (based on Co). Anal. calcd for **1** ($C_{34}H_{30}CoN_{10}O_{12}$) (%): C, 49.23; H, 3.64; N, 16.88. Found: C, 49.56; H, 3.95; N, 16.33%. IR (cm^{-1}, KBr): 3332(s), 3168(s), 3051(m), 1695(s), 1615(s), 1591(m), 1571(s), 1436(s), 1399(s), 1221(m), 1036(w), 917(w), 823(s), 720(s), 625(m).

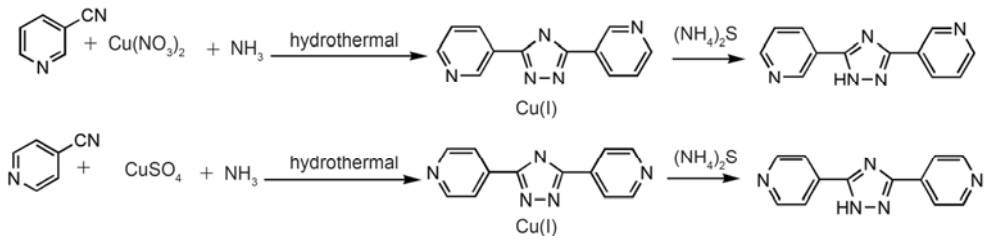

Scheme 2 *In situ* synthesis of Hbpt.

2.4 Synthesis of [Co(4,4′-Hbpt)(pm)$_{0.5}$(H$_2$O)]·3H$_2$O (2)

A mixture containing Co(OAc)$_2$·4H$_2$O (24.9 mg, 0.10 mmol), 4,4′-Hbpt (11.2 mg, 0.05 mmol), H$_4$pm (25.4 mg, 0.10 mmol) and water (6 mL) was sealed in a 15 mL Teflon-lined stainless steel vessel and heated at 160 °C for 3 days and then cooled to room temperature at a rate of 5 °C/h. Red prism crystals of **2** were collected in a yield of 55% (based on Co). Anal. calcd for **2** ($C_{17}H_{18}CoN_5O_8$): C, 42.60; H, 3.79; N, 14.61. Found: C, 42.91; H, 3.51; N, 15.15%. IR (cm^{-1}, KBr): 3396(m), 3262(s), 3088(m), 2643(w), 1604(s), 1550(s), 1485(s), 1461(s), 1403(s), 1378(s), 1225(m), 1038(w), 1060(w), 1020(s), 995(m), 952(w), 839(m), 771(m), 721(m), 704(s), 604(s), 508(m).

2.5 Synthesis of [Co(3,4′-Hbpt)(pm)$_{0.5}$(H$_2$O)$_3$]·2H$_2$O (3)

The same procedure as that for **2** was used for the synthesis of **3** except that 4,4′-Hbpt was replaced by 3,4′-Hbpt, and red prismatic crystals of **3** were collected in a yield of 30% (based on Co). Anal. calcd for **3** ($C_{17}H_{20}CoN_5O_9$): C, 41.06; H, 4.05; N, 14.08. Found: C, 41.65; H, 4.18; N, 14.85%. IR (cm^{-1}, KBr): 3332(s), 1635(s), 1615(s), 1581(m), 1544(s), 1456(s), 1399(s), 1220(m), 1036(w), 917(w), 836(s), 740(s), 720(s), 615(m).

2.6 Single crystal X-ray crystallography

All diffraction data for compounds **1–3** were collected on a Bruker SMART APEX II CCD diffractometer with graphite monochromated Mo Kα radiation (λ = 0.071073 nm) at 293(2) K. Absorption corrections were applied using SADABS [26]. All structures were solved by direct methods using SHELXS-97 [27] and refined with full-matrix least-squares refinements based on F^2 using SHELXL-97 [28]. All non-hydrogen atoms were refined anisotropically. Hydrogen atoms were placed in geometrically calculated positions. Crystallographic details for **1–3** are summarized in Table 1. Selected bond lengths and angles of the compounds are indicated in Table S1. Possible partial hydrogen bond geometries of compounds are listed in Table S2.

Table 1 Crystallographic data and structure refinement details for compounds **1–3**

Compound	**1**	**2**	**3**
Empirical formula	$C_{34}H_{30}CoN_{10}O_{12}$	$C_{17}H_{18}CoN_5O_8$	$C_{17}H_{20}CoN_5O_9$
Formula weight	829.61	479.29	497.31
Crystal system	Triclinic	Triclinic	monoclinic
Space group	$P\bar{1}$	$P\bar{1}$	$P2_1/n$
a (nm)	0.80718(10)	0.87880(13)	0.73533(5)
b (nm)	0.99614(12)	1.09939(16)	1.94938(14)
c (nm)	1.14448(14)	1.10850(17)	1.39685(10)
α (°)	110.032(2)	76.825(2)	90
β (°)	90.134(2)	77.100(2)	97.5660(10)
γ (°)	97.081(2)	67.533(2)	90
V (nm^3)	0.85699(18)	0.9525(2)	1.9849(2)
Z	1	2	4
μ (mm^{-1})	0.584	0.960	0.929
Unique reflect	3576	3334	3538
Observed reflect	4973	4804	9833
*R*int	0.0196	0.0172	0.0254
Final *R* indices [*I*>2sigma(*I*)]	*R*1 = 0.0486, *wR*2 = 0.1296	*R*1 = 0.0383, *wR*2 = 0.0957	*R*1 = 0.0407, *wR*2 = 0.1096

3 Results and discussion

3.1 Synthesis

1,2,4-triazoles and their derivatives are generally prepared by multi-step procedures, which usually involve hydrazine derivatives as starting agents [29–31]. Since *in situ* metal/ligand reactions show great merits in both coordination chemistry and organic synthesis [32–34], herein, 3,5-bispyridyl-1*H*-1,2,4-triazole has been synthesized via an *in situ* metal/ligand reaction, using a coordination compound as an intermediate. Such an approach not only represents a widely applicable nonhydrazine-based synthetic route for triazolates but also simplifies the synthesis and purification processes.

3.2 Structural analysis

Single crystal X-ray analysis shows that **1** has a one-dimensional (1D) array structure. The asymmetric unit of **1** has one crystallographically independent Co(II) center, displaying a slightly distorted octahedral geometry involving coordination to two O atoms from H_2pm^{2-}, two coordinated water molecules in the equatorial plane and two N atoms from two 3,3′-Hbpt ligands in the axial position (Figure 1(a)). The H_2pm^{2-} ligand acts as a bis(monodentate) mode to link the adjacent metal ions through its deprotonated carboxylic groups. It is worth noting that the 3,3′-Hbpt is not deprotonated, and a (4,4) topological layer is formed by the parallel 1D neighboring chains using O–H···hydrogen bonding interactions between carboxylic groups and nitrogen atoms of the 3,3′-Hbpt (Figure 1(b)).

To examine the effect of positional isomerism on the structure, **2** was synthesized in the presence of 4,4′-Hbpt. The asymmetric unit of **2** consists of a pair of Co(II) ions, one Hbpt, one coordinated water molecule, half a pyromellitate ligand, and three free water molecules (Figure 2(a)). Co1 adopts a distorted octahedral geometry with two water molecules in *trans* apical position (Co1–O5 0.2105 (25) nm), two oxygen atoms from two different monodentate carboxylate groups (Co1–O2 0.2069(18) nm) and two nitrogen atoms of two Hbpt molecules (Co1–N2 0.2186 (27) nm) in the basal plane, in which the cobalt(II) ion and the basal atoms are absolutely coplanar. Meanwhile, Co2 lies on the symmetry center, and shows an elongated octahedral coordination environment with axial Co2–N1

bonds of length 0.2163(22) nm to two Hbpt ligands, with the basal four oxygen atoms coming from two pairs of neighboring carboxylic groups (Co2–O1 0.2104(25), Co2–O4 0.2089(21) nm). In **2**, H_4pm is completely deprotonated and exhibits monodentate and bis(monodentate) coordination modes. The pm^{4-} moieties connect the Co(II) ions giving a two-dimensional (2D) layer pattern with (4,4) network topology, in which the grid size is 0.989 nm × 1.06 nm (Figure 2(b)).These sheets are further linked by Hbpt ligands along the *c* axis to form a pillared-grid three-dimensional (3D) open framework with 1D open channels. From a topological point of view, **2** can be described as a 3D NbO network with $(6^4.8^2)$ topology.

Surprisingly, there are three uncoordinated water molecules in every primary channel unit (Figure 2(c)). A calculation using PLATON [35] leads to a potential solvent area of 0.1686 nm^3 per unit cell volume of 0.9525 nm^3, namely 17.7% of the total crystal volume. In view of such a low cavity ratio, the channel is filled by free water molecules, which can be attributed to larger space occupation and the longer distance of the bi-pillar shutters [36].

3 is a 2D coordination polymer. The Co(II) ion is six-coordinated in a distorted octahedral coordination geometry by one oxygen atom from pm^{4-}, two pyridyl nitrogen atoms, and three water oxygen atoms (Figure 3(a)). The Co–O bond distances range from 0.2064(2) to 0.2135(2) nm, while the Co–N bond lengths are slightly longer, ranging from 0.2140(4) to 0.2143(2) nm. The adjacent Co(II) ions are linked together by N atoms from 3,4′-Hbpt to form a metal helical chain. Interestingly, such chains crystallize in both right- and left-handed fashions. The pm^{4-} acts as a bridge in a bis(monodentate) binding mode linking adjacent helical chains through its *para*-positioned carboxylic groups, resulting in a regular 2D architecture (Figure 3(b)).

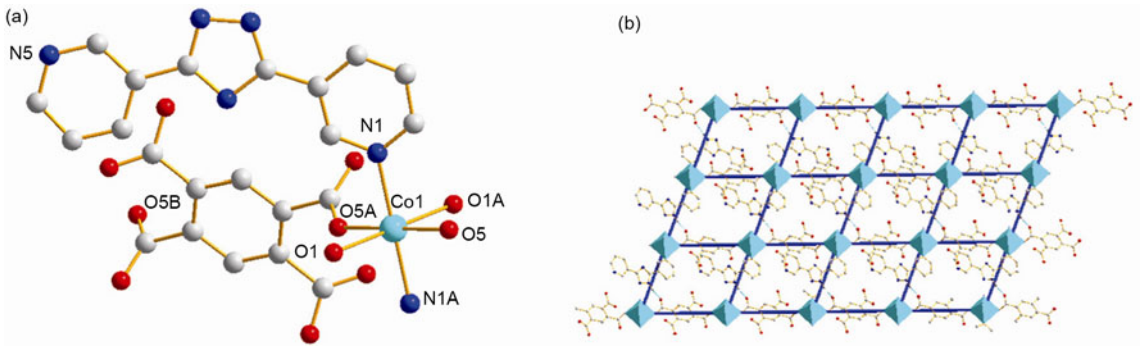

Figure 1 (a) Coordination environment of Co^{2+} in **1** (lattice water and H atoms are omitted for clarity); (b) (4,4) topological layer formed by the 1D parallel neighbor chains by using O–H···N hydrogen bonding interactions.

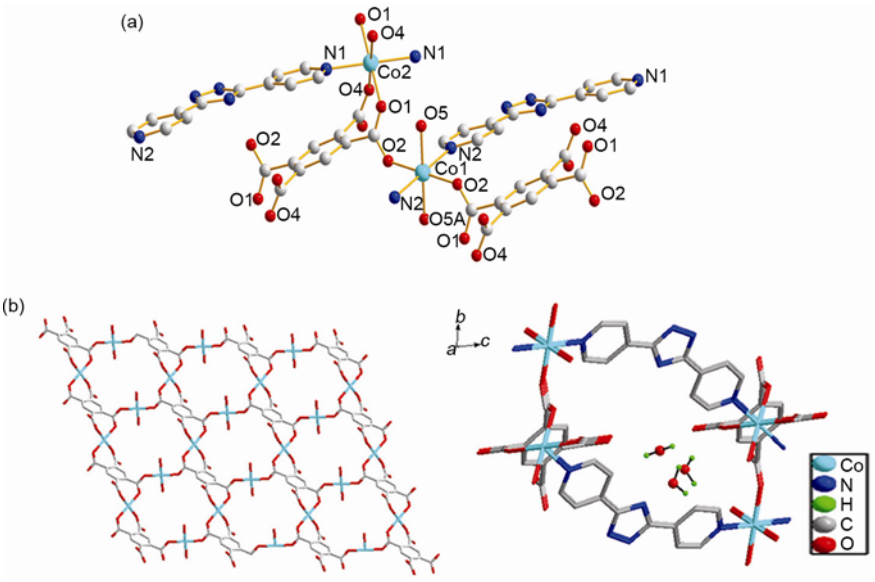

Figure 2 (a) Coordination environment of Co^{2+} in **2** (lattice water and H atoms are omitted for clarity); (b) the 2D layer extended in the *ab* plane based on pm and Co ions; (c) free water molecules encapsulated in a 1D channel along the *a* axis.

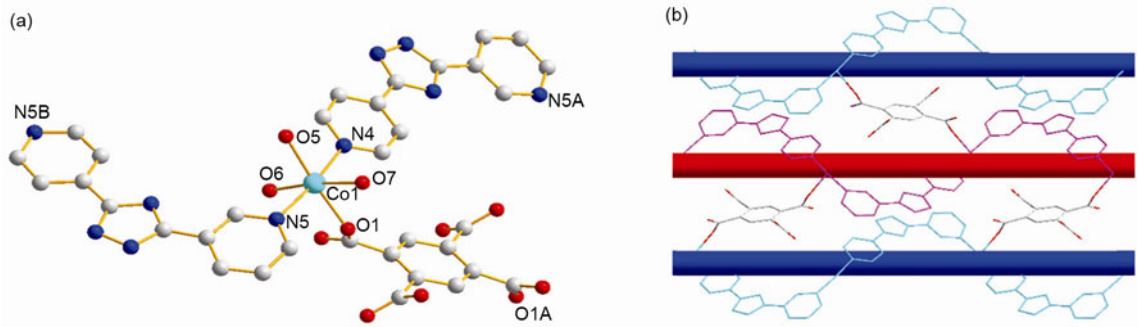

Figure 3 (a) Coordination environment of Co^{2+} in **3** (lattice water and H atoms are omitted for clarity); (b) 2D architecture assembled by both right- and left-handed helical chains.

3.3 Coordination modes for the positionally isomeric ligands

It is noteworthy that the positionally isomeric ligands in MOFs **1–3** are all neutral but still exhibit a variety of coordination modes, as illustrated in Scheme 3. Hbpt acts as monodentate and bis (monodentate) connectors. Furthermore, the triazole moiety in Hbpt is involved in strong hydrogen bonds, which contributes to the supramolecular network. It is obvious that the introduction of the auxiliary H_4pm greatly influences the final structures. The carboxylic groups adopt monodentate, chelating and bridging modes, which is mostly responsible for the structural diversity. With the variation in coordination patterns of Hbpt and H_4pm, the network arrays show 1D chains, a 2D network and a 3D framework in **1–3** respectively.

3.4 Thermal gravimetric analysis

Thermal gravimetric analyses (TGA) were carried out from 50 to 800 °C (see Figures S1–S3 for TGA curves). **1** loses lattice water at about 60 °C with a weight loss of 4.47% (calc. 4.34%), and then remains stable up to 360 °C before undergoing successive weight losses. **2** experiences consecutive weight loss steps, which do not end until 800 °C. **3** is stable up to 100 °C and then undergoes a two step weight loss of 10.2% from 100 to 360 °C, corresponding to the release of the lattice water molecules (calc. 10.8%).

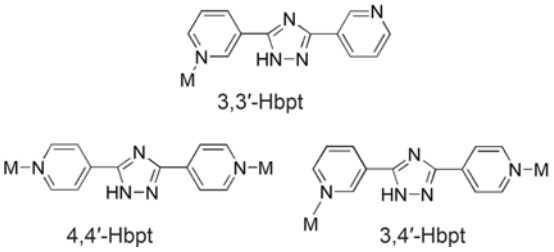

Scheme 3 Coordination modes of Hbpt.

3.5 Effects on the thermal decomposition of ammonium perchlorate

Compounds **1–3** and AP were mixed in a mass ratio of 1:3 to prepare samples for thermal decomposition analyses. The total sample mass used was less than 1.0 mg for all runs. From Figure 4, the endothermic peak at 245 °C for pure AP is due to a crystallographic transition of AP from the orthorhombic to the cubic phase. The second and third peaks for pure AP are exothermic, and correspond to the low-temperature decomposition (LTD) process and the high-temperature decomposition (HTD) process [37, 38]. The exothermic peak of the LTD process occurs at about 290 °C at a heating rate of 10 °C min^{-1}, corresponding to the decomposition of AP with a heat of 0.735 kJ g^{-1}. The exothermic peak for the HTD process is at 442 °C with a heat of 0.787 kJ g^{-1}.

The DSC curves of AP in the presence of compounds **1–3** are also shown in Figure 4. In each case, there is no effect on the crystallographic transition temperature of APP. In the presence of compound **1**, the exothermic peak occurred at 318 °C, indicating that AP is completely decomposed at a lower temperature than for pure AP. Similarly, in the presence of **2**, a sharp decomposition peak was observed at 300 °C, showing that AP is decomposed in a much shorter time than for pure AP. In the presence of compound **3**, the LTD and HTD peaks converged to 338 and 457 °C. The onsets of thermal decomposition of the pure AP and AP in the presence of compounds **1–3** were all at about 300 °C, while the end temperatures were about 490, 343, 335 and 476 °C, respectively. The thermal decomposition rate of AP in presence of compounds **1** and **2** occurs more rapidly than pure AP, while addition of compound **3** to AP reduces the rate of decomposition. Moreover, in the presence of compounds **1**, **2** and **3**, the decomposition heats are 2.58, 2.00, and 0.82 kJ g^{-1}, respectively, significantly higher than the corresponding heat value for neat AP.

It is known that the decomposition temperature is related to the heating rate (as shown in the Supporting Information). The relationship between decomposition temperature and heating rate can be described by the Kissinger correlation, as shown in eq. (1).

$$\ln\frac{\beta}{T_p^2} = \ln\frac{AR}{E_a} - \frac{E_a}{RT_p} \quad (1)$$

where E_a is the apparent activation energy, β is the heating rate, R is the gas constant, T_p is the peak temperature, and A is the pre-exponential factor. According to this equation, the values of the activation energy E_a were obtained by Kissinger's method at four different heating rates (see Figures S4–S6 for DSC curves). For pure AP, the calculated activation energy is 74.65 kJ mol^{-1}. As shown in Table 2, in presence of **1**, **2** and **3**, the activation energies increased to 170.03, 249.47 and 124.31 kJ mol^{-1}, respectively. The increase in activation energy and the corresponding increase in the A value can be attributed to the kinetic compensation effect as reported previously [39]. The ratio of $E_a/\ln(A)$ can be used to describe the reactivity [40]. Usually, a larger ratio means a much greater stability of the reactant. The ratios of $E_a/\ln(A)$ are 14.1, 13.06 ,12.13 and 14.81 for pure AP, AP with **1**, AP with **2** and AP with **3,** respectively. Obviously, **1** and **2** show a better catalytic activity toward AP decomposition than **3**, which is consistent with the single exothermic peak in the corresponding DSC curves,.

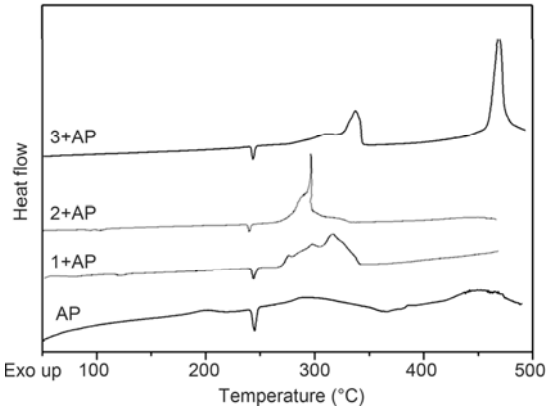

Figure 4 DSC curves for AP, **1** + AP, **2** + AP and **3**+AP.

4 Conclusion

We have demonstrated here three new Co(II) MOFs generated from mixed-ligand systems containing three positionally isomeric ligands (3,3′-Hbpt, 4,4′-Hbpt and 3,4′-Hbpt) and H_4pm under coordination-driven assembly. The introduction of H_4pm greatly influences the coordination modes of Hbpt as well as the final supramolecular structures. Moreover, the effects of the three compounds on the thermal decomposition of AP have also been studied. Compounds **1** and **2** show good catalytic performance in AP decomposition, which could make them promising energetic additives for AP-based propellants.

Table 2 Kinetic parameters of the thermal decomposition of pure AP and AP with additives (T_p and ΔH were measured at the heating rate of 10 °C min^{-1})

	T_p (°C)	ΔH (kJ g^{-1})	E_a (kJ mol^{-1})	ln[A/s]	r
AP	290	0.735	74.65	5.71	0.9830
1 +AP	318	2.582	170.03	13.01	0.9785
2 +AP	310	2.008	249.47	20.56	0.9784
3+AP	338	0.816	124.31	8.391	0.9911

This work was supported by the National Natural Science Foundation of China (21073142, 21173168 and 21127004), the Natural Science Foundation of Shaanxi Province (SJ08B09) and the Natural Science Foundation of the Department of Education of Shaanxi Province (2010JK882, 2010JQ2007 and 11JS110).

Appendix A. Supplementary material

CCDC 775294–775296 contain the supplementary crystallographic data for **1–3**. These data can be obtained free of charge from The Cambridge Crystallographic Data Centre via www.ccdc.cam.ac.uk/data_request/cif. Selected bond lengths, angles and hydrogen-bonding interactions are tabulated for **1–3**. TG curves and DSC curves are attached for compounds **1–3**, respectively.

1 Zhang JP, Lin YY, Huang XC, Chen XM. Copper(I) 1,2,4-triazolates and related compounds: Studies of the solvothermal ligand reactions, network topologies, and photoluminescence properties. *J Am Chem Soc*, 2005, 127: 5495–5506

2 Zhang JP, Lin YY, Huang XC, Chen XM. Supramolecular isomerism within three-dimensional 3-connected nets: unusual synthesis and characterization of trimorphic copper(I) 3,5-dimethyl-1,2,4-triazolate. *Dalton Trans*, 2005, 3681–3685

3 Meng X, Song Y, Hou H, Han H, Xiao B, Fan Y, Zhu Y. Hydrothermal syntheses, crystal structures, and characteristics of a series of Cd-btx coordination polymers (btx = 1,4-bis(triazol-1-ylmethyl) benzene). *Inorg Chem*, 2004, 43: 3528–3536

4 Zhang JP, Chen XM. Exceptional framework flexibility and sorption behavior of a multifunctional porous cuprous triazolate framework. *J Am Chem Soc*, 2008, 130: 6010–6017

5 Schneider CJ, Cashion JD, Moubaraki B, S. Neville M, Batten SR, Turner DR, Murray KS. The magnetic and structural elucidation of 3,5-bis(2-pyridyl)-1,2,4-triazolate-bridged dinuclear iron(II) spin crossover compounds. *Polyhedron*, 2007, 26: 1764–1772

6 Huang FP, Tian JL, Gu W, Liu X, Yan SP, Liao DZ, Cheng P. Co(II) coordination polymers: Positional isomeric effect, structural and magnetic diversification. *Cryst Growth Des*, 2010, 10: 1145–1154

7 Du M, Jiang XJ, Zhao XJ. Controllable assembly of metal-directed coordination polymers under diverse conditions: A case study of the M^{II}–H_3tma/Bpt mixed-ligand system. *Inorg Chem*, 2006, 45: 3998–4006

8 Zhai QG, Wu XY, Chen SM, Lu CZ, Yang WB. Construction of Cd/Zn(II)-1,2,4-triazolate coordination compounds via changing substituents and anions. *Cryst Growth Des*, 2006, 6: 2126–2135

9 Xue H, Gao Y, Twamley B, Shreeve JNM. New energetic salts based on nitrogen-containing heterocycles. *Chem Mater*, 2005, 17: 191–198

10 Haasnoot JG. Mononuclear, oligonuclear and polynuclear metal coordination compounds with 1,2,4-triazole derivatives as ligands. *Coord Chem Rev*, 2000, 200–202: 131–185

11 Kulkarni PB, Reddy TS, Nair JK, Nazare AN, Talawar MB, Mukundan T, Asthana SN. Studies on salts of 3-nitro-1,2,4-triazol-5-one (NTO) and 2,4,6-trinitroanilinobenzoic acid (TABA): Potential energetic ballistic modifiers. *J Hazard Mater*, 2005, 123: 54–60

12 Zhao FQ, Xue L, Xing XL, Hu RZ, Zhou ZM, Gao HX, Yi JH, Xu SY, Pei Q. Thermochemical properties and thermokinetic behavior of energetic triazole ionic salts. *Sci Chin Chem*, 2011, 54: 461–474

13 Pschirer NG, Ciurtin DM, Smith MD, Bunz UHF, Loye HCZ. Noninterpenetrating square-grid coordination polymers with dimensions of 25 × 25 $Å^2$ prepared by using *N*,*N*′-type ligands: The first chiral square-grid coordination polymer. *Angew Chem Int Ed*, 2002, 41: 583–585

14 Brandys M, Puddephatt R. Ring, polymer and network structures in silver(I) compounds with dipyridyl and diphosphine ligands. *Chem Commun*, 2001, 1508–1509

15 Huang FP, Tian JL, Gu W, Yan SP. Three 3D Cu(II) coordination polymers constructed from 1,2,4,5-benzenetetracarboxylate acid and three positional isomeric ligands. *Inorg Chem Commun*, 2010, 13: 90–94

16 Chen LJ, Li LP, Li GS. Synthesis of CuO nanorods and their catalytic activity in the thermal decomposition of ammonium perchlorate. *J Alloys Compd*, 2008, 464: 532–536

17 Ping C, Li F, Jian Z, Wei J. Preparation of Cu/CNT composite particles and catalytic performance on thermal decomposition of ammonium perchlorate. *Pyrotech*, 2006, 31: 452–455

18 Yu ZX, Chen LF, Lu LD, Yang XJ, Wang X. DSC/TG-MS study on *in situ* catalytic thermal decomposition of ammonium perchlorate over CoC_2O_4. *Chin J Catal*, 2009, 30: 19–23

19 Klapötke TM, Minar NK, Stierstorfer J. Investigations of bis(methyltetrazolyl)triazenes as nitrogen-rich ingredients in solid rocket propellants—synthesis, characterization and properties. *Polyhedron*, 2009, 28: 13–26

20 Oommen C, Jain SR. Ammonium nitrate: A promising rocket propellant oxidizer. *J Hazard Mater*, 1999, A67: 253–281

21 D'Andrea B, Lillo F, Faure A, Perut C. A new generation of solid propellants for space launchers. *Acta Astronautica*, 2000, 47: 103–112

22 Sun D, Cao R, Liang Y, Shi Q, Hong M. Syntheses, crystal structures and properties of two novel lanthanide–carboxylate polymeric compounds. *Dalton Trans*, 2002: 1847–1851

23 Kumagai H, Kepert CJ, Kurmoo M. Construction of hydrogen-bonded and coordination-bonded networks of cobalt(II) with pyromellitate: Synthesis, structures, and magnetic properties. *Inorg Chem*, 2002, 41: 3410–3422

24 Cheng D, Khan MA, Houser RP. Novel sandwich coordination polymers composed of cobalt(II), 1,2,4,5-benzenetetracarboxylato ligands, and homopiperazonium cations. *Cryst Growth Des*, 2002, 2: 415–420

25 Browne E. 1,2,4-Triazol-3-ylpyridines. *Aust J Chem*, 1975, 28: 2543–2546

26 Sheldrick, GM. SADABS: Program for Empirical Absorption Correction of Area Detector Data; University of Göttingen: Göttingen, Germany, 1996

27 Sheldrick, GM. SHELXS-97, Program for Solution of Crystal Structures, University of Göttingen: Göttingen, Germany, 1997

28 Sheldrick, GM. SHELXL-97, Program for Refinement of Crystal Structures, University of Göttingen: Göttingen, Germany, 1997

29 Klingele MH, Boyd PDW, Moubaraki B, Murray KS, Brooker S. Probing the dinucleating behaviour of a bis-bidentate ligand: Synthesis and characterization of some di- and mononuclear cobalt(II), nickel(II), copper(II) and zinc(II) compounds of 3,5-di(2-pyridyl)-4-(1H-pyrrol-1-yl)-4H-1,2,4-triazole. *Eur J Inorg Chem*, 2006, 573–589

30 Zumbrunn A. The first versatile synthesis of 1-alkyl-3-fluoro-1H-[1,2,4]triazoles. *Synthesis*, 1998, 1357–1361

31 Kitchen JA, White NG, Boyd M, Moubaraki B, Murray KS, Boyd PDW, Brooker S. Iron(II) tris-[N4-substituted-3,5-di(2-pyridyl)-1,2,4-triazole] compounds: Structural, magnetic, NMR, and density functional theory studies. *Inorg Chem*, 2009, 48: 6670–6679

32 Blake A, Champness N, Chung S, Li W, Schrder M. *In situ* ligand synthesis and construction of an unprecedented three-dimensional array with silver(I): A new approach to inorganic crystal engineering. *Chem Commun*, 1997, 1675–1676

33 Chen XM, Tong ML. Solvothermal *in situ* metal/ligand reactions: A new bridge between coordination chemistry and organic synthetic

chemistry. *Acc Chem Res*, 2007, 40: 162–170
34 Xie XF, Chen SP, Xia ZQ, Gao SL. Construction of metal–organic frameworks with transitional metals based on the 3,5-bis(4-pyridyl)-1H-1,2,4-triazole ligand. *Polyhedron*, 2009, 28: 679–688
35 Spek AL. PLATON, a multipurpose crystallographic tool, Utrecht University, 1999
36 Wen GL, Wang YY, Liu P, Guo CY, Zhang WH, Shi QZ. Construction of metal–organic frameworks with transitional metals based on the 3,5-bis(4-pyridyl)-1H-1,2,4-triazole ligand. *Inorg Chim Acta*, 2009, 362: 1730–1738
37 Lang AJ, Vyazovkin S. Effect of pressure and sample type on decomposition of ammonium perchlorate. *Combust. Flame*, 2006, 145: 779–790
38 Vyazovkin S, Wight CA. Kinetics of thermal decomposition of cubic ammonium perchlorate. *Chem Mater*, 1999, 11: 3386–3393
39 Brill TB, Gongwer PE, Williams GK. Thermal decomposition of energetic materials. 66. Kinetic compensation effects in HMX, RDX, and NTO. *J Phys Chem*, 1994, 98: 12242–12247
40 Andričić B, Kovačić T, Klarić IT. Kinetic analysis of the thermooxidative degradation of poly(vinyl chloride) in poly(vinyl chloride)/methyl methacrylate–butadiene–styrene blends 2. Nonisothermal degradation. *Polym Degrad Stab*, 2003, 79: 265–270